Chemosphere 254 (2020) 126916

Contents lists available at ScienceDirect

Chemosphere

journal homepage: www.elsevier.com/locate/chemosphere

Biochar derived from red algae for efficient remediation of 4-nonylphenol from marine sediments

Chang-Mao Hung [a], C.P. Huang [b], Shu-Ling Hsieh [c], Mei-Ling Tsai [c], Chiu-Wen Chen [a, **], Cheng-Di Dong [a, *]

[a] Department of Marine Environmental Engineering, National Kaohsiung University of Science and Technology, Kaohsiung City, Taiwan
[b] Department of Civil and Environmental Engineering, University of Delaware, Newark, USA
[c] Department of Seafood Science, National Kaohsiung University of Science and Technology, Kaohsiung City, Taiwan

HIGHLIGHTS

- RAB was successfully prepared from red algae biomass.
- Real marine sediments were treated with SPC oxidation for 4-NP removal.
- Calcium-enriched RAB efficiently activated SPC to generate reactive radicals.
- pH and RAB dose controlled 4-NP degradation.
- Langmuir-Hinshelwood model described well the kinetics of 4-NP degradation.

GRAPHICAL ABSTRACT

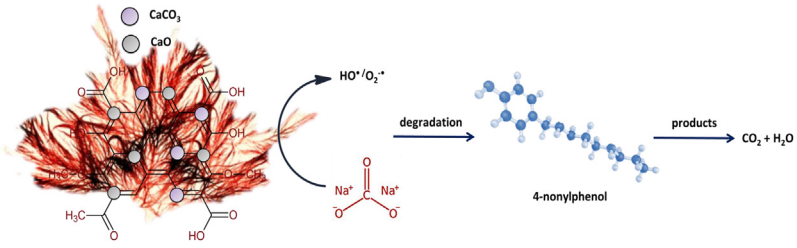

ARTICLE INFO

Article history:
Received 12 February 2020
Received in revised form
21 April 2020
Accepted 25 April 2020
Available online 29 April 2020

Handling Editor: Veeriah (Jega) Jegatheesan

Keywords:
Red algae
Biochar
Sodium percarbonate
4-Nonylphenol
Sediments

ABSTRACT

4-Nonylphenol (4-NP), a phenolic endocrine disruptor chemical (EDC), is known to have high toxicity to aquatic organisms and humans. The remediation of 4-NP-contaminated marine sediments was studied using red algae-based biochar (RAB) thermochemically synthesized from *Agardhiella subulata* with simple pyrolysis process under different temperatures of 300–900 °C in CO_2 atmosphere. The RAB was characterized by XRD, Raman, FTIR spectroscopy, and zeta potential measurements. The calcium in RAB efficiently activated sodium percarbonate (SPC) to generate reactive radicals for the catalytic degradation of 4-NP at pH 9.0. The oxygen-containing functional groups reacted with H_2O_2, which increased the generation of reactive radicals under alkaline pH condition. Ca^{2+} ion was the active species responsible for 4-NP degradation. $CaO/CaCO_3$ on RAB surface enhanced direct electron transfer, increased HO• production, and 4-NP degradation in marine sediments. Langmuir–Hinshelwood type kinetics well described the 4-NP degradation process. Remediation of contaminated sediments using RAB could be a sustainable approach toward closed-loop biomass cycling in the degradation of 4-NP contaminants.

1. Introduction

The frequent presence of nonylphenol ethoxylate (NPEO), nonionic surfactant discharged from various anthropogenic sources such as household, industrial, and agricultural activities, in marine and freshwater ecosystems is one of the most common emerging substances of concern (ESOC) in the sediments (Fang et al., 2019;

* Corresponding author.
** Corresponding author.
E-mail addresses: cwchen@nkust.edu.tw (C.-W. Chen), cddong@nkust.edu.tw (C.-D. Dong).

https://doi.org/10.1016/j.chemosphere.2020.126916
0045-6535/

Wang et al., 2019). 4-Nonylphenol (4-NP) is a metabolite of NPEO, which is more recalcitrant than its parent compound. 4-NP is an important environmental phenolic endocrine disruptor chemical (EDC) and an indicator of seafood contamination (Chang et al., 2019; Zhou et al., 2019). At elevated concentrations in different environmental systems such as reservoirs, rivers, lakes, wetlands, streams, and marine matrices, 4-NP exhibited high toxicity, in terms of estrogenic activity and teratogenicity, to aquatic organisms and humans (Gong et al., 2019). Effective techniques such as bioremediation and advanced oxidation process (AOP) for 4-NP degradation are urgently needed to safeguard ecological and human health (Hussain et al., 2017; Dong et al., 2019a; Kent and Tay, 2019; Mtibaà et al., 2020).

AOP is effective in oxidizing and mineralizing many toxic and biorefractory organic compounds due to of high oxidation potential from possible reactive oxygen species (ROS) (Qi et al., 2013; Hung et al., 2016a,b; Danish et al., 2017; Dong et al., 2018a,b; 2019a,b; Dong et al., 2020). Among all HO• generation systems, sodium percarbonate ($2Na_2CO_3 \cdot 3H_2O_2$, SPC), a solid carrier of hydrogen peroxide (H_2O_2), can produce oxidizing species, i.e. hydroxyl (HO•) and superoxide anion (O_2^{-}•) radicals, which exhibit strong oxidation ability toward the degradation of organic contaminants (Cravotto et al., 2007). SPC is alkaline and has high pH buffer capacity over a wide pH range (Fu et al., 2015). Zuo et al. (2020) reported that the degradation of carbamazepine (CBZ) in wastewater by radical-based (specifically, HO• and SO_4^{-}•) techniques using microwave-ultraviolet catalyzed oxidation systems followed the order: SPC > H_2O_2 > persulfate (PS) > peroxymonosulfate (PMS). SPC is a strong oxidant capable of removing a wide list of refractory contaminants. Cravotto et al. (2007) studied the treatment of *p*-nonylphenol (NP) by SPC under microwave (MW) irradiation. Miao et al. (2015) used hydroxylamine hydrochloride modified Fe-catalyzed SPC process to enhance the removal of tetrachloroethene (PCE). The Fe(III)/Fe(II) redox couple, yielding a relatively steady Fe(II) and higher of HO•/O_2^{-}• radicals, which resulted in almost complete PCE removal. Moreover, Cui et al. (2017) studied ethylbenzene (EB) removal in aqueous solutions by SPC oxidation over (S,S)-ethylenediamine-N,N-disuccinic acid (EDDS)—Fe(III) catalyst and complete oxidation occurred at pH 5.5 in 90 min and HO• was the predominant species responsible for EB degradation. Farooq et al. (2017) investigated the degradation of trichloroethane (TCA) by SPC over binary Fe—Cu/reduced graphene oxide (rGO). Results showed that the combination of Fe and Cu supported on rGO greatly enhanced TCA degradation because of high surface area (119.2 m^2/g) that provided more active sites for the generation of ROS in the SPC system. Additionally, Chen et al. (2018) studied the degradation of Rhodamine B (RhB) dye by SPC over iron oxychloride (FeOCl) catalyst under visible light (FeOCl/SPC/Vis) and reported that the degradation of RhB increased with active iron sites. Although above studies have addressed the issue that combining SPC with catalyst can enhance the degradation efficiency of organic contaminants synergistically, but high cost of metallic catalysts, leaching of metal ions, incomplete removal of the organic contamination, and the formation of the toxic byproducts still remain engineering challenges (De Luna et al., 2020). Therefore, it is necessary to develop eco-friendly and cost-effective bio–based materials, such as biochar, as SPC activators to produce radicals, i.e., HO• and O_2^{-}•, for improving the degradation efficiency of hazardous chemicals.

Biochar is a highly porous material rich in varying surface functional groups, polarity and crystallinity. However, feedstock, thermos-chemical process and pretreatment of biomass and post treatment of biocahr determined the surface heterogeneity and thus reactivity. Del Bubba et al. (2020) studied the adsorption of 4-t-octylphenol (4-t-OP) and 4-nonyphenol (4-NP) on a wide list of biochars prepared from wide list of biomaterials and pyrolysis temperature and reported that pyrolysis temperature was the most influential parameter on surface properties and thus reactivity of biochar.

Algae are main primary producers in most ecosystems. Algae, both autotrophic and heterotrophic, which biomass contains proteins, polysaccharides and lipids, are capable of generating substantial biomass (Duan et al., 2019). The potential benefits of marine algal biomass, both microalgae and macroalgae, as algal-based foods, phycocolloids, biomedicinals, fertilizers, biofuels, soil amendment, and nutrient scavengers in wastewater treatment systems, in terms of circular bioeconomy framework, has received increasing attention in recent years (Alobwede et al., 2019; Amin and Chetpattananondh, 2019; Jaafari and Yaghmaeian, 2019a,b; Thivya and Vijayaraghavan, 2019; Nagarajan et al., 2020).De Bhowmick et al. (2018)De Bhowmick et al., 2018 reported that microalgae could be grown in wastewater for simultaneous production of high-value products and biochar. Red algal (*Agardhiella subulata*) is a common bioresource with that can be produced at large quantity rapidly. The algal biomass can be used to produce polysaccharides, such as agars or carrageenan, valuable gelling and stabilizing reagents for pharmaceutical applications (Murnao et al., 1997; Rorrer and Cheney, 2004; Sudhakar et al., 2018). De Bhowmick et al. (2019)De BhowmickSarmah and Sen, 2019 reported that algae will be next generation feedstock. Algal biomass can be environmentally sustainable material for the production of biochar catalyst, an attractive option to enhance the capacity of remediating contaminated waters and soils (Roberts et al., 2015). Moreover, the alkaline nature of algal biochar can be ideal acid soils conditioner and the inorganic ash components, namely, P, K, Mg and Ca, can be beneficial soil amendments to enhance crop productivity (Yu et al., 2017). One potential end-use of algal biomass, especially, the fast-growing calcium oxide-rich red algae, is for the production of biochar (Bird et al., 2011; Sharma et al., 2019). Red algal is a potential Ca source that is suitable for the preparation of Ca-modified biochar for use as heterogeneous catalyst. Moreover, calcium is an alkaline earth metal ion having weak Lewis acidity due to its small electronegativity (Bazargan et al., 2015). Hence, calcium ion contributes to high activity in transesterification reaction during biodiesel production, and enhances adsorption phosphate due to its high basicity (Wang et al., 2019; Liu et al., 2019). This study aims at the preparation, characterization and applications of red algal biochar as catalyst for the degradation of refractory contaminants in sediments. We have previously studied the treatment of PAHs and 4-NP contaminated sediments using bamboo biochar modified by Fe_3O_4 (Dong et al., 2017, 2019c). To the best of our knowledge, the preparation and testing of calcium oxide-rich macroalgal biochar, in one-step pyrolysis, for SPC activation toward the remediation of 4-NP-contaminated sediments has not yet been studied. Major factors, such as pyrolysis temperature, SPC and RAB dosages, and pH affecting the kinetics of 4-NP degradation were investigated.

2. Materials and methods

2.1. Sediment samples

Sediment samples were collected from the Jen-Gen River, Kaohsiung City, Taiwan (longitude 120°18.12′ E, latitude 22°35.13′ N). The samples were immediately placed in pre-cleaned amber bottles (with Teflon gasket and screw cap) upon dredging. The collected sediments were frozen while being transported to the laboratory. The samples were air-dried at room temperature and

then freeze-dried for 72 h prior to laboratory experiments. The sand, silt, and clay content of typical sediment samples were 24, 68, and 8%, respectively.

2.2. Chemicals

Chemicals used included sodium percarbonate ($2Na_2CO_3 \cdot 3H_2O_2$, SPC) (20–30% H_2O_2) from Sigma-Aldrich Co. Ltd. (St. Louis, USA), acetone, methanol, dichloromethane, and *n*-hexane (99.8% purity, HPLC grade) from Echo Chemical Co., Ltd. (Miaoli, Taiwan), 4-nonylphenols ($C_{15}H_{24}O$, NP) and branched side-chain-mixed compounds (99.5% purity) from Tokyo Kasei Kogyo Co., Ltd. (Tokyo, Japan), and internal standard (p-terphenyl, 99.5% purity) from Chem Service Inc. (Pennsylvania, U.S.A). The above reagents were of analytical grade. The biochar was produced by the pyrolysis of red algae (*Agardhiella subulata*) as raw biomass material. Red algae samples were provided by Po-Wu Botechnology Co. Ltd (Pingtung, Taiwan). The collected red algae was washed several times with deionized water to remove the epiphytes, microbes, sand particles, and other impurities, dried in air for 1 h, again at 60 °C in oven for 24 h, then dried algae material was ground to powder form. The powdered red algae was pyrolyzed at temperature ranging from 300 to 900 °C and heating rate of 10 °C min^{-1} in a furnace in CO_2 atmosphere to produce red algae biochar (RAB). The RAB was washed thoroughly, oven-dried at 60 °C for 24 h, and then stored in a desiccator for future use. The solid products was denoted as RAB300, RAB500, RAB700, and RAB900, for pyrolysis temperature of 300, 500, 700 and 900 °C, respectively. Raw red algae had a CaO content of about 734 mg g^{-1} reported previously (Su et al., 2014).

2.3. 4-NP degradation experiments

All experiments were conducted at room temperature (303 K). To 40-mL borosilicate glass vial, it was added 1 g of dry sediment sample, 1.0–5.0 g L^{-1} of RAB, and 25 mL of solution containing SPC and 4-NP at molar ratio of 1–1000 : 1. Then all sample vials were gently shaken for 30 s before placing in a water bath shaker (SB-9D, Taiwan Hipoint Corporation, Kaohsiung, Taiwan) and continuingly shaken at a speed of 200 rpm for 6 h. At the end of preselected time interval, i.e., 1–6 h, the solution was quenched with methanol to terminate the oxidation reaction. Then the sediment slurry was extracted for residual 4-NP with dichloromethane to determine the amount of 4-NP degraded. The 4-NP concentration was detected using gas chromatography–mass spectrometry (GC–MS) (Agilent 6890 N GC/5975 MS). The initial solution pH was adjusted with HCl (0.1 M) and NaOH (0.1 M) to the desired value. Parameters such as dosage of RAB and pH on 4-NP degradation were investigated. Each degradation experiment was performed in triplicate.

2.4. Chemical analyses

XRD analysis was performed using a Diano-8536 diffractometer equipped with CuKα radiation source. Raman spectroscopy analysis was conducted using a visible Raman system (Nanofinder 30, Tokyo Instruments, Japan) with a 632.8 nm He–Ne laser. Fourier transform infrared (FTIR) spectra were collected in the range of 400–4000 cm^{-1} with FTIR spectrometer (FT-700, Horiba, Japan) using potassium bromide (KBr) pellet. Zeta potential of the catalyst was measured with Zetasizer Nano ZS90 (Malvern Instruments, Worcestershire, UK). The suspension pH was adjusted from pH 3 to 11 using 0.1 M of HNO_3 or 0.1 M of NaOH. The 4-NP concentration was analyzed using GC–MS. The transfer line and ion source temperature were 280 and 230 °C, respectively. The 4-NP was separated using an HP-5MS (30 m × 0.25 mm i. d. × 0.25 μm film thickness) capillary column (Hewlett-Packard, Palo Alto, CA, USA). Helium was the carrier gas at a flow rate of 1.5 mL min^{-1}. The GC oven temperature was initially set to 70 °C for 2 min, increased to 240 °C at 20 °C min^{-1}, then to 300 °C at 5 °C min^{-1}, and finally maintained at 300 °C for 5 min. The mass spectrometer was operated in selected ion monitoring (SIM) mode. The 4-NP concentration was quantified based on the internal standard method. The final concentration was corrected based on the recovery. The results showed remarkable repeatability and reproducibility of 4-NP measurement.

3. Results and discussion

3.1. Characterization of RAB

The XRD peaks of typical graphite-like crystalline carbon in RAB were at $2\theta = 25.9°$ and 43.9°, which were characteristic of (002) and (100) planes (Fig. 1a). Significant CaO peaks of were at $2\theta = 31.6°$, 36.3°, 47.3°, 52.9°, and 64.1°, which were corresponding to the lattice planes (111), (200), (220), and (222) (Liu et al., 2019). The XRD peaks of RAB appeared at $2\theta = 23.0°$, 29.4°, 35.9°, 43.2°, 47.5°, 48.5°, 57.4°, 60.6°, and 64.6°, representing the lattice planes of (012), (104), (110), (202), (018), (116), (122), (119), and (300) of $CaCO_3$ (Chang et al., 2011). The results showed the presence of CaO and $CaCO_3$ in RAB900, along with low intensity peaks of graphite-like structures, which suggested that RAB was carbonated with CO_2 and $CaCO_3$ was formed. However, moisture and CO_2 easily reacted with CaO to form $Ca(OH)_2$ and $CaCO_3$, respectively. These inactive phases could reduce the activity and basicity of RAB (Wang et al., 2019). CO_2 reacted with CaO and $Ca(OH)_2$ to form a thermodynamically stable $CaCO_3$ according to Eqs. (1) and (2). CO_2 acted as an activation agent and generated a large number of small porous structures in biochar (Shi et al., 2020). As the pyrolysis temperature increased from 700 to 900 °C, the intensity of CaO and $CaCO_3$ peaks increased gradually while the intensity of C peaks decreased sharply, due to the chemical reaction between CaO and graphite-like phases and the coverage of RAB by CaO and $CaCO_3$.

$$CaO_{(s)} + CO_2 \rightarrow CaCO_{3(s)} \quad (1)$$

$$Ca(OH)_{2(s)} + CO_2 \rightarrow CaCO_{3(s)} + H_2O \quad (2)$$

Raman analysis provides more information about the surface properties of RAB (Fig. 1b). The peaks in the region of 1360 cm^{-1} corresponding to D bands (carbon sp^3 hybridization) and peaks in the range of 1586 cm^{-1} was associated with the G bands (carbon sp^2 hybridization). The results of the FTIR analyses for RAB, obtained in the wavenumber region between 4000 and 400 cm^{-1}, which indicated changes in their surface functional groups in relation to the different pyrolysis temperatures for the positive or negative catalytic effects of RAB for the degradation of 4-NP (Fig. 1c). The samples exhibited these peaks at 1470, 689, and 907 cm^{-1}, representing the asymmetric stretch modes of Ca–O bonds, respectively (Wang et al., 2019). Moreover, three peaks were observed at 1385, 1160, and 1040 cm^{-1} corresponding to the O–H stretching in the plane of free hydroxyl groups, surface C–O–C, and C–O bonds, respectively (Shi et al., 2020). The peak at 1430 cm^{-1} was assigned to the antisymmetric stretching of carboxylic acid (–COOH) and carboxylate (–COO–) groups in RAB due to aromatic ring modes, which were important to maintain hydrophilicity of catalyst. The band of the C=O group appeared at 1556 cm^{-1}. The band at 1100 cm^{-1} corresponded to the polysaccharide rings and became most prominent at higher temperature (Bird et al., 2011). The increase in band intensity of oxygen-containing functional groups (OFGs) was observed for RAB900,

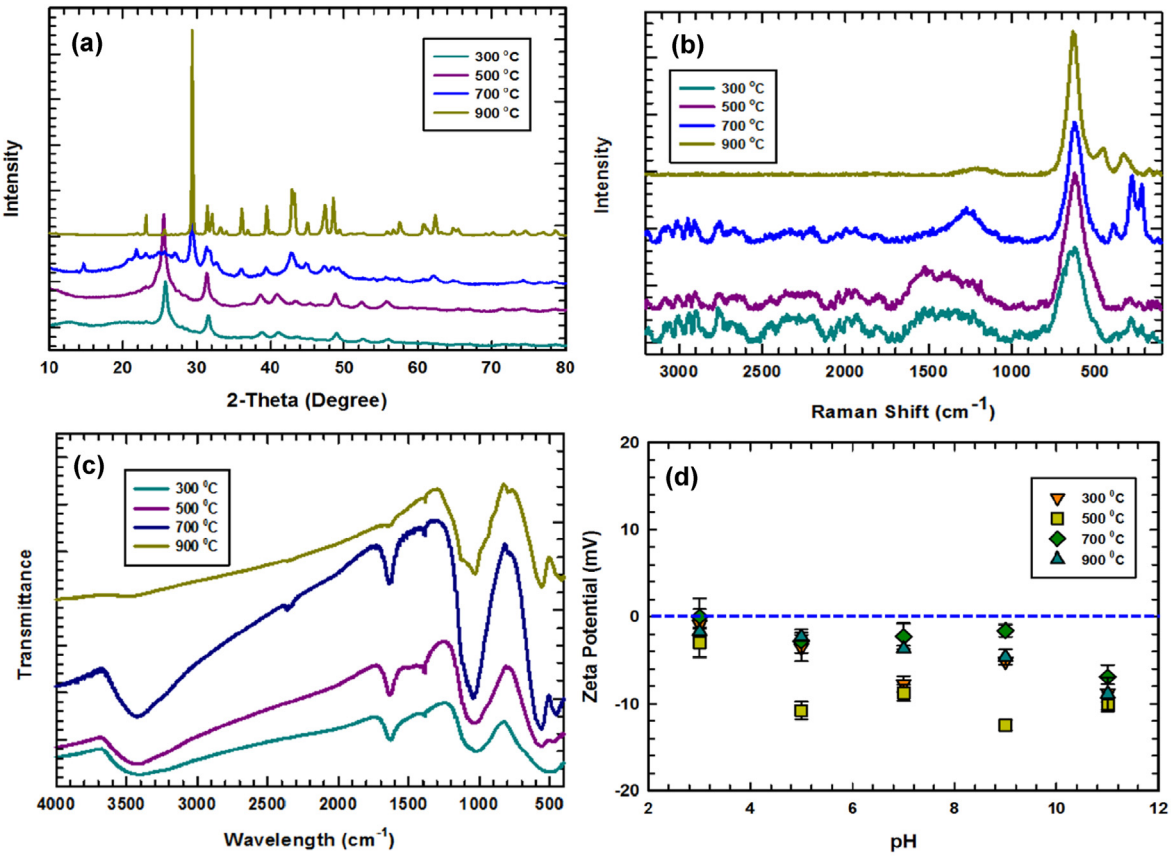

Fig. 1. The (a) XRD pattern, (b) Raman, (c) FTIR and (d) zeta potential of RAB catalyst.

which provided information on the surface functionalization process. Poo et al. (2018) reported that the OFG density of marine macro-algae biochar was larger than that of woody biochar. Therefore, OFGs were active catalytic sites and electron acceptors for the oxidation of 4-NP. In addition, the RAB surface charge was determined by zeta potential measurements over the pH range of 3–11 to further explore the catalytic mechanism (Fig. 1d). The zeta potential of RAB900 was approximately −24 mV at pH 3 and decreased to −39 mV at pH 11, which clearly indicated that RAB was negatively charged. Electronic interactions between 4-NP and RAB might play a role on the adsorption and the catalytic activity of RAB. This behavior could be attributed, in part, to surface functionalization; that is, OFGs, including –COO–, –COOH, and –OH, onto the RAB surface thus decreased the surface potential. Results of zeta potential and FTIR analyses suggested that 4-NP degradation over RAB involved electrostatic attraction and hydrophobic interactions between 4-NP and OFGs. FTIR results confirmed the successful deposition of CaO phase on to the carbon framework through Ca–O–C linkages between CaO and porous carbon support. The formation of Ca–O–C bond enhanced the stability of the Ca-based composite catalysts and reduced the loss of Ca^{2+} ions (Wang et al., 2019). Thus, results of the XRD, Raman, and FTIR clearly indicated the presence of CaO on RAB surface.

3.2. The activity of RAB toward 4-NP degradation

The 4-NP concentration observed in sediments was approximately 56,136 ± 7342 ng g^{-1} dry weight (dw). Fig. 2a shows the degradation of 4-NP as affected by SPC concentration. Results show less than 5% loss of 4-NP in the absence of SPC. 4-NP degradation increased significantly at higher SPC concentration. At the highest SPC concentration of 2×10^{-2} M (or Σ[4-NP] to [SPC] molar ratio of 1:1000), Σ4-NP removal reached 75%. Results indicated that adequate SPC must be available to produce of HO• radicals for 4-NP degradation. As shown in Fig. 2b, Σ[4-NP]/[SPC] ratio of 1:1000 gave rate constant, k_{obs}, of 9.9×10^{-2} h^{-1}, which was almost 3.7 times that 2.7×10^{-2} h^{-1} of Σ[4-NP]/[SPC] ratio 1:1. After reaction, SPC was converted to bicarbonate and carbonate ions (HCO_3^- and CO_3^{2-}), which might scavenge HO• and O_2^-• to form carbonate radical (CO_3^-•) (Gao et al., 2020). CO_3^-• could react with the aromatic substrates through an electrophilic addition, substitution, or direct electron transfer reaction but at a lower rate than HO• (Miao et al., 2015; Cui et al., 2017). Therefore, 2×10^{-4} M (at Σ[4-NP]/[SPC] molar ratio of 1:10) was selected as the optimal reaction concentration and used for further study.

Further experiments were conducted to examine 4-NP degradation by SPC on RAB prepared at different pyrolysis temperature. The results showed that RAB900 effectively activated SPC, to yield a maximum 4-NP degradation of 67%, which was greater than that of SPC (47%) alone (Fig. 3a). The findings demonstrated that RAB played a critical role toward 4-NP degradation owing to the synergistic effects exhibited by CaO and the porous carbon support of biochar. Yin et al. (2013) reported that natural CaO-rich sepiolite calcined at 900 °C exhibited remarkable phosphorus removal capacity. Furthermore, high calcination temperature could significantly govern the formation of graphitized carbon skeleton of biochar, which resulted in high surface functionality and porosity (Liu et al., 2015). Therefore, the role of RAB in the RAB/SPC system included direct decomposition of SPC and accelerating SPC oxidation mediated by reactive Ca-phases. Therefore, CaO, the main

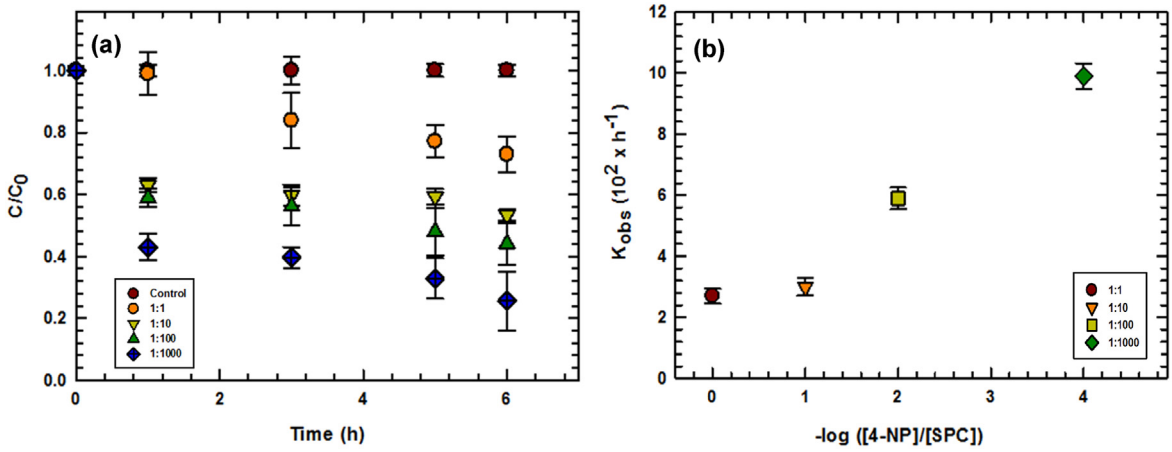

Fig. 2. (a) Effect of percarbonate concentration and (b) rate constant of 4-NP degradation. Experimental conditions: sediment = 1.00 g, reaction volume = 40 mL, T = 30 °C, pH_0 = 9.0, ∑[4-NP]: [SPC] (molar ratio) = 1: 10^0–10^3.

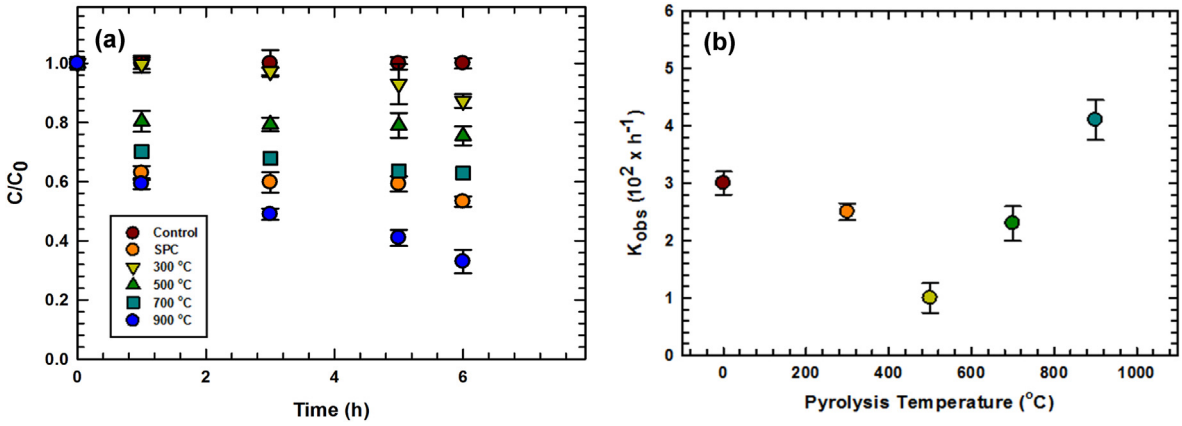

Fig. 3. (a) Effect of pyrolysis temperature of the RAB and (b) rate constant of 4-NP degradation. Experimental conditions: sediment = 1.00 g, reaction volume = 40 mL, T = 30 °C, pH_0 = 9.0, [RAB] = 3.0 g L^{-1}, [SPC] = 2 × 10^{-4} M, ∑[4-NP]: [SPC] (molar ratio) = 1 : 10.

active mineral phase, provided sufficient catalytic sites with sufficient amount of Ca^{2+} ions to facilitate the electron transfer reaction at the RAB surface toward catalytic 4-NP decomposition. The catalytic activity of CaO was derived from the basic sites and spatial dispersion defining Ca^{2+} availability (Marinković et al., 2016). The basic sites quickly reacted with ambient H_2O and CO_2 to form O^{2-} and initiated base-catalyzed reaction. Efficient electron transfer process among 4-NP, SPC, and the RAB network via Ca^{2+} (Eq. (3)), initiated the oxidation-reduction reaction to generate ROS (Granados et al., 2007).

$$CaO \leftrightarrow Ca^{2+} + O^{2-} \quad (3)$$

Moreover, the presence of OFGs on the RAB surface, such as electron-rich groups of hydroxyl (−OH) and carboxyl (−COOH) enhanced the generation of HO• according to the following reactions (Eqs. (4)–(6)), the outcome of which enhanced 4-NP degradation.

$$RAB{-}OH + H_2O_2 \rightarrow RAB{-}O^{\bullet} + HO^{\bullet} + H_2O \quad (4)$$

$$RAB{-}OOH + H_2O_2 \rightarrow RAB{-}OO^{\bullet} + HO^{\bullet} + H_2O \quad (5)$$

$$RAB{-}OOH + H_2O_2 \rightarrow RAB{-}OH + H_2O + O_2 \quad (6)$$

Sharma et al. (2019) reported that high specific surface area, porosity, and OFGs of the algal biomass effectively promoted the adsorption/photocatalytic of organic pollutants from the aqueous medium. The degradation of 4-NP oxidation by SPC over the RAB catalyst followed the pseudo-first-order kinetics. The rate constant (k_{obs}) was determined from the slope of linear ln (C/C_0) vs. time (t) plot, where C_0 and C are the 4-NP concentration at initial (t = 0) and at time t, respectively (Fig. 3b). The k_{obs} were 2.5 × 10^{-2}, 1.0 × 10^{-2}, 2.3 × 10^{-2}, and 4.1 × 10^{-2} h^{-1} for RAB300, RAB500, RAB700, and RAB900, respectively. The results revealed that the RAB900/SPC process achieved the highest 4-NP degradation rate with respect to SPC at pH 9.0. Therefore, RAB and HO• exhibited a synergistic effect on 4-NP degradation. Further study is needed still on the effect of calcium content of RAB as a function of pyrolysis temperature and how calcium ion may govern the catalytic activity of RAB during field applications.

The degradation of 4-NP was evaluated at different RAB900 dosage from 1.0 to 5.0 g L^{-1}, while keeping constant the concentration of SPC at 2 × 10^{-4} M and initial pH at 9.0 (Fig. 4a). Specifically, results showed that 3.0 g L^{-1} of RAB was able to generate enough HO• for effective degradation of 4-NP with a maximum conversion of 67%. However, higher dosage (5.0 g L^{-1}) decreased 4-NP degradation due to excess generation of H_2O_2, the higher RAB dosage enabled the graphitic structure and OFGs to scavenge the radicals and subsequently decreased the catalytic activity. The

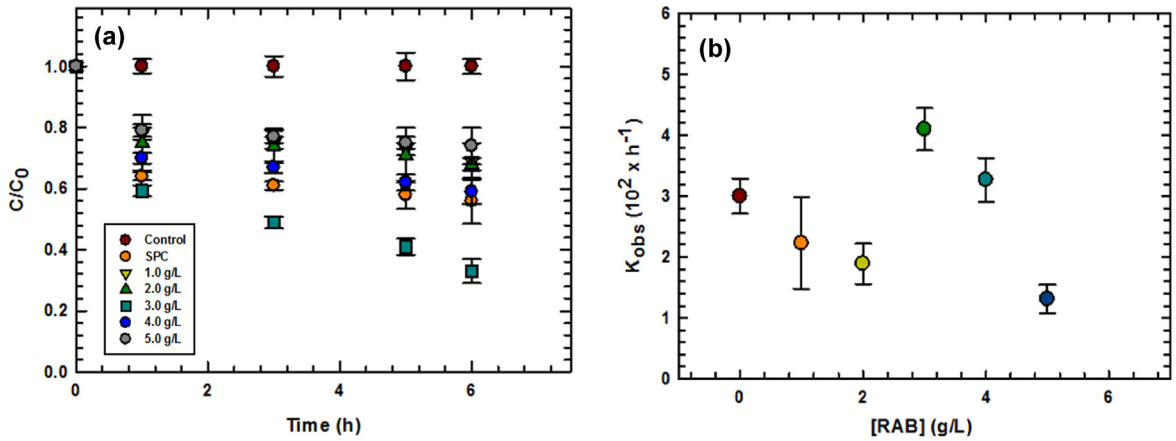

Fig. 4. (a) Effect of RAB dosage and (b) rate constant of 4-NP degradation. Experimental conditions: sediment = 1.00 g, reaction volume = 40 mL, T = 30 °C, pH_0 = 9.0, [SPC] = 2×10^{-4} M, ∑[4-NP]: [SPC] (molar ratio) = 1 : 10.

optimum 4-NP degradation rate must be achieved at a suitable RAB dose. Reaction between HO• and organic pollutants was regousible for the degradation of the later by H_2O_2 oxidation (Wang et al., 2019). Ruan et al. (2019) proposed that biochar effectively activated H_2O_2 to produce environmentally persistent free radicals (EPFRs), such as, oxygen-, carbon-, and oxygenated carbon-centered radicals, which are powerful and promising oxidants for the degradation of organic contaminants. Nevertheless, the decomposition of 4-NP in the RAB/SPC system increased with the amount of HO• due to increasing direct electron transfer between the constituents of the CaO/$CaCO_3$ oxide surface and target contaminants. Moreover, the k_{obs} were 2.2×10^{-2}, 1.9×10^{-2}, 4.1×10^{-2}, 3.3×10^{-2}, and 1.3×10^{-2} h^{-1} at RAB dosages of 1.0, 2.0, 3.0, 4.0, and 5.0 g L^{-1}, respectively (Fig. 4b). The increase in the reaction rate with increasing RAB dosage could be ascribed to the increased availability of SPC for reaction with Ca^{2+} in solution to produce a large amount of HO• for the oxidation of 4-NP. According to the Langmuir-Hinshelwood mechanism of heterogeneous catalysis reaction, rapid adsorption of reactants, i.e., SPC and 4-NP onto the catalyst surface was the first reaction step (Dobaradaran et al., 2018; Dong et al., 2019d). Accordingly, at the onset of the reaction, SPC and 4-NP adsorbs onto the active site, S_A and S_B, respectively, as showing in the following reactions:

$$S_A + SPC \rightleftharpoons S_A - SPC; \quad K_1 \tag{7}$$

$$S_B + 4 - NP \rightleftharpoons S_B - PAE; \quad K_2 \tag{8}$$

where K_1 and K_2 are the equilibrium adsorption constants of SPC and 4-NP on the different active sites of the RAB, respectively. S_A-SPC and S_B-4-NP are the adsorbed SPC and 4-NP species on the RAB surface, respectively. The reaction between the adsorbed SPC and 4-NP species is assumed the rate-limiting step, that is:

$$S_A - SPC + S_B - 4 - NP \rightarrow products + S_A + S_B; k_3 \quad (rate - limiting \ \ step) \tag{9}$$

From Eq. (9), one can obtain the following rate expression:

$$rate \ \ (r) = -\frac{d[4-NP]}{dt} = k_3 \ \ [S_A - SPC][S_B - 4 - NP] \tag{10}$$

where k_3 is the reaction rate constant. From Eqs. (7) and (8), one has:

$$[S_A - SPC] = K_1[S_A][SPC] \tag{11a}$$

and

$$[S_B - 4 - NP] = K_2[S_B][4 - NP] \tag{11b}$$

The mass balance relationship gives the following equations:

$$S^T = S_A^T + S_B^T \tag{12}$$

$$S_A^T = [S_A] + [S_A - SPC] \tag{13a}$$

and

$$S_B^T = [S_B] + [S_B - 4 - NP] \tag{13b}$$

Combing Eq. (11a) and Eq. (13a), and Eq. (11b) and Eq. (13b) gives:

$$[S_A - SPC] = \frac{S_A^T K_1[SPC]}{1 + K_1[SPC]} \tag{14a}$$

and

$$[S_B - 4 - NP] = \frac{S_B^T K_2[4 - NP]}{1 + K_2[4 - NP]} \tag{14b}$$

By substituting Eqs. (14a) and (14b) into Eq. (10), the reaction rate expression becomes:

$$r = -\frac{d[4-NP]}{dt} = k_3 \times \frac{S_A^T K_1[SPC]}{1 + K_1[SPC]} \times \frac{S_B^T K_2[4 - NP]}{1 + K_2[4 - NP]} \tag{15}$$

If $1 \gg K_1$ [SPC] and $1 \gg K_2$ [4-NP], Eq. (15) becomes:

$$r = k_3 S_A^T K_1[SPC] S_B^T K_2[4 - NP] = k_{app}[SPC][4 - NP] \tag{16}$$

where k_{app} = k3SATK1 [SPC]SBTK2. At a constant SPC concentration and [SPC] $\gg$ [4-NP], the catalytic oxidation of 4-NP follows the pseudo-first-order kinetics, as follows:

$$r = k_{obs}[4 - NP] \tag{17}$$

where $k_{obs} = k_{app}$ [SPC].

Note that k_{obs} is a function of the product of S_A and S_B. By expressing both sites as a function of the total surface sites, S_T, as θ_A

and θ_B, where $\theta_A + \theta_B = 1$, one can obtain:

$$k_{obs} \propto S_T^2 \ \theta_A \theta_B = S_T^2(1-\theta_A)\theta_A \quad (18)$$

Eq. (18) predicts that k_{obs} as a function of RAB dosage with a maximum k_{obs} near $\theta_A = \theta_B = 0.5$. Therefore it is expected that the rate constant will be at the maximum when the surface site for the specific adsorption of SPC and 4-NP are equal. Fig. 4b shows that the maximum k_{obs} was at RAB dosage of 3.0 g L^{-1}, which agreed well with Eq. (18).

The degradation of 4-NP in the RAB/SPC system was evaluated at different initial pH value (3.0, 6.0, 9.0, and 11.0). The as well degradation percent 4-NP followed the order: pH 9.0 (67%) > pH 11.0 (49%) > pH 3.0 (46%) > pH 6.0 (44%) (Fig. 5a). SPC need to replace H_2O_2 for the chemical oxidation of 4-NP in this study. SPC, having similar function as liquid H_2O_2, released free H_2O_2 into the solution when SPC was in contact with water (Eq. (19a)), which initiated a series of reaction forming several reactive species (Eqs. 19b-19i). Bicarbonate is believed to be a hydroxyl radical scavenger in the aqueous phase via reactions as shown in Eqs. 19j-19k. HCO_4^- can be generated through the equilibrium reaction between HCO_3^- and H_2O_2 in aqueous solution, as shown in Eq. 19l-19m (Fu et al., 2015). SPC, as a weak Brønsted base, raised the solution pH upon its introduction to the sediment matrix. CO_3^{2-} from SPC or inherently present in natural or slightly alkaline water systems could compete for HO• radicals with the organic contaminants. It has been reported that CO_3^{-}• was more stable at near-neutral pH than acidic (Cui et al., 2017). The initial solution pH in the RAB/SPC system was 9.0, therefore the amount of CO_3^{-}• in this system would be rather small. Thus, it was concluded that the effect of CO_3^{-}• on 4-NP degradation might be insignificant in the present system. Moreover, pH significantly affected the activity of SPC during the generation of ROS such as •OH, O_2^{-}•, and HO_2•, according to the following reactions (Miao et al., 2015; Lin et al., 2017).

$$2Na_2CO_3 \cdot 3H_2O_2 \rightarrow 2Na_2CO_3 + 3H_2O_2 \quad (19a)$$

$$2H_2O_2 \rightarrow 2H_2O + O_2 \quad (19b)$$

$$H_2O_2 \rightarrow HO_2^{\bullet} + H^+ \quad (19c)$$

$$HO_2^{\bullet} \rightarrow O_2^{-\bullet} + H^+ \quad (19d)$$

$$O_2^{-\bullet} + 2H_2O \rightarrow H_2O_2 + O_2 + H^+ \quad (19e)$$

$$H_2O_2 \rightarrow HO^{\bullet} + OH^- \quad (19f)$$

$$HO^{\bullet} + HO^{\bullet} \rightarrow H_2O_2 \quad (19g)$$

$$H_2O_2 + HO^{\bullet} \rightarrow HO_2^{\bullet} + H_2O \quad (19h)$$

$$HO_2^{\bullet} + HO^{\bullet} \rightarrow O_2 + H_2O \quad (19i)$$

$$HCO_3^- + HO^{\bullet} \rightarrow CO_3^{-\bullet} + H_2O \quad (19j)$$

$$CO_3^{-\bullet} + H_2O_2 \rightarrow HO_2^{\bullet} + HCO_3^- \quad (19k)$$

$$HCO_3^- + H_2O_2 \rightarrow HCO_4^- + H_2O \quad (19l)$$

$$HCO_4^- \rightarrow CO_3^{-\bullet} + HO^{\bullet} \quad (19m)$$

$$4\text{-NP} + HO^{\bullet} + O_2^{-\bullet} + O_2 \rightarrow \text{byproducts} + CO_2 + H_2O \quad (19n)$$

Furthermore, more HO• would be formed due to the increases in dissolution of Ca^{2+} from the alkaline calcareous RAB, which enhanced the activation of SPC, under alkaline conditions (Granados et al., 2007). The results confirmed that alkaline conditions were more reactive than acidic conditions, which was consistent with the results of other reports on 4-NP degradation (Dong et al., 2019c). Moreover, the biochar surface had the capacity to activate SPC toward HO• generation even in the absence of CaO because of the presence of C—OOH and C—OH groups on RAB surface acting as electron shuttle to mediate electron transfer reactions between the CaO constituent on the RAB surface and target contaminants in marine sediments (Hussain et al., 2017). Further, the pH of algal biochar increased with increase in pyrolysis temperature, which increased the relative ash content in the biochar and raised the pH of biochar, especially under severe pyrolysis conditions (Yu et al., 2017). The pH value significantly affected the degradation 4-NP due to the synergistic effect exhibited by RAB and HO•. The results agreed with these reported for other pollutants studied previously (Dong et al., 2018a, 2019c; Naghipour et al., 2018). The rate constant, k_{obs}, was 3.6 × 10^{-2}, 1.4 × 10^{-2}, 4.1 × 10^{-2} and 3.7 × 10^{-2} h^{-1} for pH_0 of 3.0, 6.0, 9.0 and 11.0, respectively (Fig. 5b). The results highlighted the crucial role of initial pH in governing the degradation efficiency and rate of 4-NP by SPC over RAB. It was noted that SPC functioned as Fenton-like chemistry over a wide pH range. Further investigation on the relationship between the physicochemical properties and stability and/or reusability of RAB, and the deactivation mechanisms of the

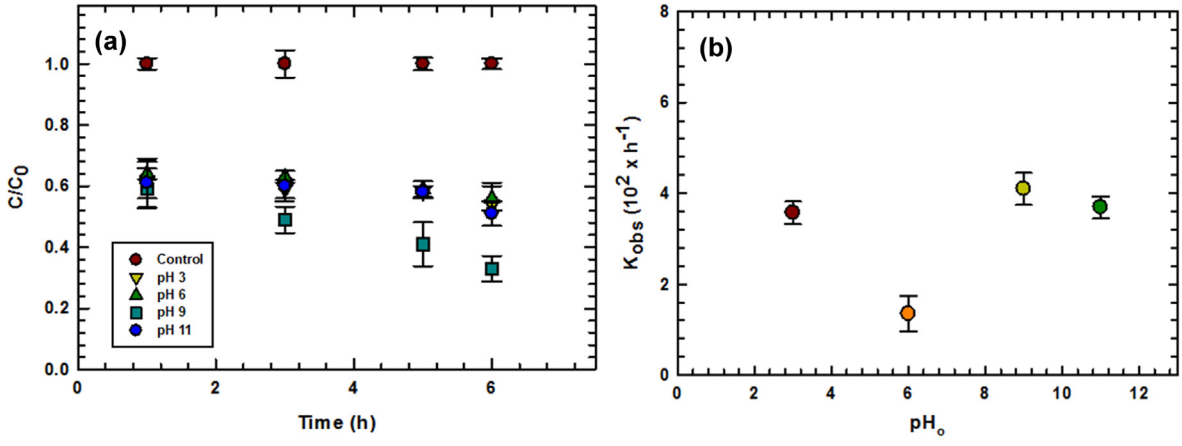

Fig. 5. (a) Effect of pH and (b) rate constant of 4-NP degradation. Experimental conditions: sediment = 1.00 g, reaction volume = 40 mL, T = 30 °C, [RAB] = 3.0 g L^{-1}, [SPC] = 2 × 10^{-4} M, ∑[4-NP]: [SPC] (molar ratio) = 1 : 10.

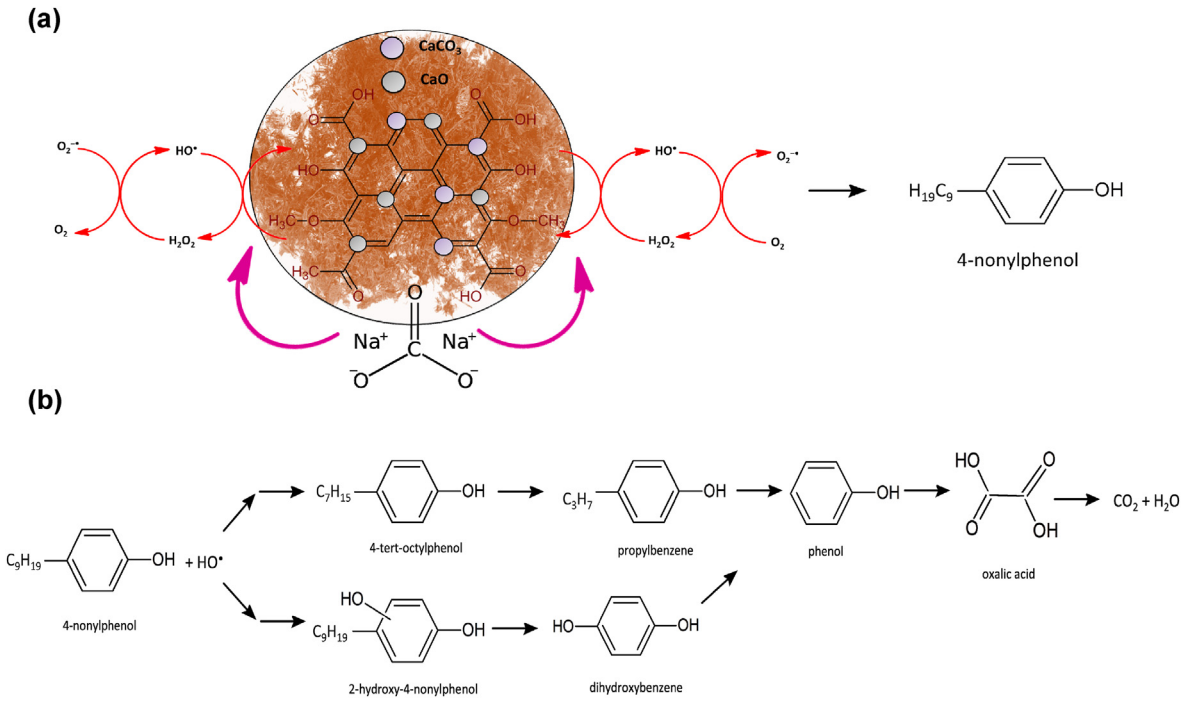

Fig. 6. (a) Proposed degradation mechanism of 4-nonylphenol (4-NP) over RAB catalyst and (b) reaction pathways of 4-NP in the sulfate and hydroxyl radical-based advanced oxidation processes.

fresh and used RAB for the degradation of 4-NP as a function of reaction time is ongoing.

3.3. Reaction mechanism of 4-NP degradation

The activation of SPC mediated by RAB was complex, owing to the presence of numeral radicals including HO• and O_2^-• and that the most oxidation reaction was electrophilic addition of HO• to aromatic rings (Fu et al., 2015). The presence of Ca^{2+} in catalyst implies the formation of oxygen vacancy, which is adsorption site for O_2 to form active chemisorbed oxygen over the calcium-based sorbent surface (Guo et al., 2018). Thus, further experiments must carried out to detect O_2^-• and HO• present the solution surface analysis techniques such by electron paramagnetic resonance spectroscopy (EPR) in the future. Furthermore, a conceptual reaction scheme was proposed to describe the degradation of 4-NP in marine sediments by activation SPC over RAB (Fig. 6a). Reaction of SPC with organic compounds produced harmless compounds, viz. CO_2, H_2O and a small amount of CO_3^{2-}, which was naturally occurring in the aquatic environment. It is generally recognized that HO• is the most active free radical in conventional Fenton system, while O_2^-• may also contribute to the degradation of contaminant to some less extent (Lin et al., 2017). RAB activated SPC to produce HO•. The CaO/$CaCO_3$ on RAB enabled efficient electron transfer between the HO• radical and 4-NP, which further transferred electron to activate SPC and HO• production. Further, reaction between HO• and H_2O formed SPC, which was strong oxidation agent. Fig. 6b shows the proposed degradation pathway of 4-NP, based on intermediates identified previously and mechanistic on the interactions between HO• and benzene rings by a series of hydroxylation of the benzene ring, cleavage of the ester bond and cleavage of one side chain (Xin et al., 2014; Xu et al., 2016). The HO• generated from the activation of SPC attacked the aromatic hydrocarbons by the electrophilic addition on the C=C double bonds of aromatic ring of 4-NP, leading to hydroxylation with the production of 4-tert-octylphenol and 2-hydroxy-4-nonylphenol. Then 4-tert-octylphenol was attacked by radicals and decomposed to propylbenzene; dealkylation of propylbenzene led to formation of phenol. Finally, phenol was oxidized with subsequent ring-opening to oxalic acid, and then CO_2 and H_2O. Moreover, 2-hydroxy-4-nonylphenol was attacked by radicals at its aromatic ring and alkyl chain to form dihydroxybenzene. Further attack on dihydroxybenzene by HO• formed phenol, which was oxidized to oxalic acid, and finally to CO_2 and H_2O, a well-reported reaction mechanism stated above. Therefore, further investigation of associated reaction byproducts from RAB/SPC treatment of 4-NP should be explored in order to better understand the health risk in the future.

4. Conclusions

RAB was prepared from the red algae raw material for 4-NP degradation in the presence of SPC. The main active mineral phase of CaO provided sufficient catalytic sites with sufficient amount of Ca^{2+} ions to facilitate the electron transfer reaction at the RAB surface toward catalytic 4-NP decomposition. Pseudo-first-order kinetics described well 4-NP degradation in the RAB/SPC system. The degradation of 4-NP was pH-dependent, maximum dependent rate at pH 9.0. The degradation mechanism might be dominated by the electrostatic attraction and hydrophobic interactions between 4-NP and OFGs on the RAB surface. Results demonstrated that coupling calcium with algal-derived materials can be a sustainable technology for closed-loop biomass cycling in the decomposition of 4-NP pollutants from marine sediments.

Declaration of competing interests

The authors declare that they have no known competing financial interests or personal relationships that could have appeared to influence the work reported in this paper.

CRediT authorship contribution statement

Chang-Mao Hung: Conceptualization, Methodology, Investigation, Validation, Formal analysis, Writing - original draft. **C.P. Huang:** Writing - review & editing, Visualization. **Shu-Ling Hsieh:** Resources. **Mei-Ling Tsai:** Resources. **Chiu-Wen Chen:** Resources. **Cheng-Di Dong:** Resources, Supervision.

Acknowledgments

The authors would like to thank the Ministry of Science and Technology of Taiwan, for financial support to perform this study under Contract Nos. MOST 106-2221-E-022-002-MY3, 106-2221-E-022-003-MY3 and 108-2221-E-992-051-MY3. Addition support was provided by US NSF IOA (1632899) to CPH.

References

Alobwede, E., Leake, J.R., Pandhal, J., 2019. Circular economy fertilization: testing micro and macro algal species as soil improvers and nutrient sources for crop production in greenhouse and field conditions. Geoderma 334, 113–123.

Amin, M., Chetpattananondh, P., 2019. Biochar from extracted marine Chlorella sp. residue for high efficiency adsorption with ultrasonication to remove Cr(VI), Zn(II) and Ni(II). Bioresour. Technol. 289, 121578–121587.

Bazargan, A., Kostić, M.D., Stamenković, O.S., Veljković, V.B., McKay, G., 2015. A calcium oxide-based catalyst derived from palm kernel shell gasification residues for biodiesel production. Fuel 150, 519–525.

Bird, M.I., Wurster, C.M., de Paula Silva, P.H., Bass, A.M., de Nys, R., 2011. Algal biochar – production and properties. Bioresour. Technol. 102, 1886–1891.

Chang, E.E., Chen, C.H., Chen, Y.H., Pan, S.Y., Chiang, P.C., 2011. Performance evaluation for carbonation of steel-making slags in a slurry reactor. J. Hazard Mater. 186, 558–564.

Chang, W.H., Liu, S.C., Chen, H.L., Lee, C.C., 2019. Dietary intake of 4-nonylphenol and bisphenol A in Taiwanese population: integrated risk assessment based on probabilistic and sensitive approach. Environ. Pollut. 244, 143–152.

Chen, M., Xu, H., Wang, Q., Li, D., Xia, D., 2018. Activation mechanism of sodium percarbonate by FeOCl under visible-light-enhanced catalytic oxidation. Chem. Phys. Lett. 706, 415–420.

Cravotto, G., Carlo, S.D., Ondruschka, B., Tumiatti, V., Roggero, C.M., 2007. Decontamination of soil containing POPs by the combined action of solid Fenton-like reagents and microwaves. Chemosphere 69, 1326–1329.

Cui, H., Gu, X., Lu, S., Fu, X., Zhang, X., Fu, G.Y., Qiu, Z., Sui, Q., 2017. Degradation of ethylbenzene in aqueous solution by sodium percarbonate activated with EDDS–Fe(III) complex. Chem. Eng. J. 309, 80–88.

Danish, M., Gu, X., Lu, S., Brusseau, M.L., Ahmad, A., Naqvi, M., Farooq, U., Zaman, W.Q., Fu, X., Miao, Z., 2017. An efficient catalytic degradation of trichloroethene in a percarbonatesystem catalyzed by ultra-fine heterogeneous zeolite supported zerovalent iron-nickel bimetallic composite. Appl. Catal., A: Gen. 531, 177–186.

De Bhowmick, G., Sarmah, A.K., Sen, R., 2018. Lignocellulosic biorefinery as a model for sustainable development of biofuels and value added products. Bioresour. Technol. 247, 1144–1154.

De Bhowmick, G., Sarmah, A.K., Sen, R., 2019. Zero-waste algal biorefinery for bioenergy and biochar: a green leap towards achieving energy and environmental sustainability. Sci. Total Environ. 650, 2467–2482.

De Luna, M.D.G., Sablas, M.M., Hung, C.M., Chen, C.W., Garcia-Segura, S., Dong, C.D., 2020. Modeling and optimization of imidacloprid degradation by catalytic percarbonate oxidation using artificial neural network and Box-Behnken experimental design. Chemosphere 251, 126254.

Del Bubba, M., Anichini, B., Bakari, Z., Bruzzoniti, M.C., Camisa, R., Caprini, C., Checchini, L., Fibbi, D., Ghadraoui, A.E., Liguori, F., Orlandini, S., 2020. Physico-chemical properties and sorption capacities of sawdust-based biochars and commercial activated carbons towards ethoxylated alkylphenols and their phenolic metabolites in effluent wastewater from a textile district. Sci. Total Environ. 708, 135217.

Dobaradaran, S., Nodehi, R.N., Yaghmaeian, K., Jaafari, J., Niari, M.H., Bharti, A.K., Agarwal, S., Gupta, V.K., Azari, A., Shariatifar, N., 2018. Catalytic decomposition of 2-chlorophenol using an ultrasonic-assisted Fe_3O_4–TiO_2@MWCNT system: influence factors, pathway and mechanism study. J. Colloid Interface Sci. 512, 172–189.

Dong, C.D., Chen, C.W., Hung, C.M., 2017. Synthesis of magnetic biochar from bamboo biomass to activate persulfate for the removal of polycyclic aromatic hydrocarbons in marine sediments. Bioresour. Technol. 245, 188–195.

Dong, C.D., Chen, C.W., Kao, C.M., Chien, C.C., Hung, C.M., 2018a. Wood-biochar-supported magnetite nanoparticles for remediation of PAH-contaminated estuary sediment. Catalysts 8, 73–86.

Dong, C.D., Tsai, M.L., Chen, C.W., Hung, C.M., 2018b. Remediation and cytotoxicity study of polycyclic aromatic hydrocarbon-contaminated marine sediments using synthesized iron oxide–carbon composite. Environ. Sci. Pollut. Res. 6, 5243–5253.

Dong, C.D., Lu, Y.C., Chang, J.H., Wang, T.H., Chen, C.W., Hung, C.M., 2019a. Enhanced persulfate degradation of PAH-contaminated sediments using magnetic carbon microspheres as the catalyst substrate. Process Saf. Environ. Protect. 125, 219–227.

Dong, C.D., Chen, C.W., Hung, C.M., 2019b. Persulfate activation with rice-husk-based magnetic biochar for degrading PAEs in marine sediments. Environ. Sci. Pollut. Res. 26, 33781–33790.

Dong, C.D., Chen, C.W., Tsai, M.L., Chang, J.H., Lyu, S.Y., Hung, C.M., 2019c. Degradation of 4-Nonylphenol in marine sediments by persulfate over magnetically modified biochars. Bioresour. Technol. 281, 143–148.

Dong, C.D., Huang, C.P., Nguyen, T.B., Hsiung, C.F., Wu, C.H., Lin, Y.L., Chen, C.W., Hung, C.M., 2019d. The degradation of phthalate esters in marine sediments by persulfate over iron–cerium oxide catalyst. Sci. Total Environ. 696, 133973–133982.

Dong, C.D., Chen, C.W., Nguyen, T.B., Huang, C.P., Hung, C.M., 2020. Degradation of phthalate esters in marine sediments by persulfate over Fe–Ce/biochar composites. Chem. Eng. J. 384, 123301.

Duan, X., Chen, Y., Yan, Y., Feng, L., Chen, Y., Zhou, Q., 2019. New method for algae comprehensive utilization: algae-derived biochar enhances algae anaerobic fermentation for short-chain fatty acids production. Bioresour. Technol. 289, 121637–121644.

Fang, J.J., Wang, S., Tang, J.P., Zhao, J.L., Wang, L., Wang, J.X., Liu, S.L., Li, F., Long, S.X., Yang, Y., 2019. Bioaccumulation of endocrine disrupting compounds in fish with different feeding habits along the largest subtropical river, China. Environ. Pollut. 247, 999–1008.

Farooq, U., Danish, M., Lu, S., Brusseau, M.L., Naqvi, M., Fu, X., Zhang, X., Sui, Q., Qiu, Z., 2017. Efficient transformation in characteristics of cations supported-reduced graphene oxide nanocomposites for the destruction of trichloroethane. Appl. Catal., A: Gen. 544, 10–20.

Fu, X., Gu, X., Lu, S., Miao, Z., Xu, M., Zhang, X., Qiu, Z., Sui, Q., 2015. Benzene depletion by Fe^{2+}-catalyzed sodium percarbonate in aqueous solution. Chem. Eng. J. 267, 25–33.

Gao, J., Duan, X., O'Shea, K., Dionysiou, D.D., 2020. Degradation and transformation of bisphenol A in UV/Sodium percarbonate: dual role of carbonate radical anion. Water Res. 171, 115394.

Gong, J., Ran, Y., Zhang, D., Chen, D., Li, H., Huang, Y., 2019. Vertical profiles and distributions of aqueous endocrine-disrupting chemicals in different matrices from the Pearl River Delta and the influence of environmental factors. Environ. Pollut. 246, 328–335.

Granados, M.L., Poves, M.D.Z., Alonso, D.M., Mariscal, R., Galisteo, F.C., Moreno-Tost, R., Santamaría, J., Fierro, J.L.G., 2007. Biodiesel from sunflower oil by using activated calcium oxide. Appl. Catal. B Environ. 73, 317–326.

Guo, H., Kou, X., Zhao, Y., Wang, S., Sun, Q., Ma, X., 2018. Effect of synergistic interaction between Ce and Mn on the CO_2 capture of calcium-based sorbent: textural properties, electron donation, and oxygen vacancy. Chem. Eng. J. 334, 237–246.

Hung, C.M., Chen, C.W., Jhuang, Y.J., Dong, C.D., 2016a. Fe_3O_4 magnetic nanoparticles: characterization and performance exemplified by the degradation of methylene blue in the presence of persulfate. J. Adv. Oxid. Technol. 19, 43–51.

Hung, C.M., Chen, C.W., Liu, Y.Y., Dong, C.D., 2016b. Decolorization of methylene blue by persulfate activated with FeO magnetic particles. Water Environ. Res. 88, 675–686.

Hussain, I., Li, M., Zhang, Y., Li, Y., Huang, S., Du, X., Liu, G., Hayat, W., Anwar, N., 2017. Insights into the mechanism of persulfate activation with nZVI/BC nanocomposite for the degradation of nonylphenol. Chem. Eng. J. 311, 163–172.

Jaafari, J., Yaghmaeian, K., 2019a. Optimization of heavy metal biosorption onto freshwater algae (*Chlorella coloniales*) using response surface methodology (RSM). Chemosphere 217, 447–455.

Jaafari, J., Yaghmaeian, K., 2019b. Response surface methodological approach for optimizing heavy metal biosorption by the blue-green alga *Chroococcus disperses*. Desalination Water Treat 142, 225–234.

Kent, J., Tay, J.H., 2019. Treatment of 17α-ethinylestradiol, 4-nonylphenol, and carbamazepine in wastewater using an aerobic granular sludge sequencing batch reactor. Sci. Total Environ. 652, 1270–1278.

Lin, K.Y.A., Lin, J.T., Lin, Y.F., 2017. Heterogeneous catalytic activation of percarbonate by ferrocene for degradation of toxic amaranth dye in water. J. Taiwan Inst. Chem. Eng. 78, 144–149.

Liu, W.J., Jiang, H., Yu, H.Q., 2015. Development of biochar-based functional materials: toward a sustainable platform carbon material. Chem. Rev. 115, 12251–12285.

Liu, X., Shen, F., Qi, X., 2019. Adsorption recovery of phosphate from aqueous solution by CaO-biochar composites prepared from eggshell and rice straw. Sci. Total Environ. 666, 694–702.

Marinković, D.M., Stanković, M.V., Veličković, A.V., Avramović, J.M., Miladinović, M.R., Stamenković, O.O., Veljković, V.B., 2016. Calcium oxide as a promising heterogeneous catalyst for biodiesel production: current state and perspectives. Renew. Sustain. Energy Rev. 56, 1387–1408.

Miao, Z., Gu, X., Lu, S., Brusseau, M.L., Yan, N., Qiu, Z., Sui, Q., 2015. Enhancement effects of reducing agents on the degradation oftetrachloroethene in the Fe(II)/Fe(III) catalyzed percarbonate system. J. Hazard Mater. 300, 530–537.

Mtibaà, R., Ezzanad, A., Aranda, E., Pozo, C., Ghariani, B., Moraga, J., Nasri, M., Cantoral, J.M., Garrido, C., Mechichi, T., 2020. Biodegradation and toxicity reduction of nonylphenol, 4-*tert*-octylphenol and 2,4-dichlorophenol by the ascomycetous fungus *Thielavia* sp HJ22: identification of fungal metabolites and

proposal of a putative pathway. Sci. Total Environ. 708, 135129.
Murnao, E., Toffanin, R., Cecere, E., Rizzo, R., Knutsen, S.H., 1997. I nvestigation of the carrageenans extracted from *Solieria filiformis* and *Agardhiella subulata* from Mar Piccolo, Taranto. Mar. Chem. 58, 319–325.
Nagarajan, D., Lee, D.J., Chen, C.Y., Chang, J.S., 2020. Resource recovery from wastewaters using microalgae-based approaches: a circular bioeconomy perspective. Bioresour. Technol. 302, 122817.
Naghipour, D., Taghavi, K., Ashournia, M., Jaafari, J., Movarrekh, R.A., 2018. A study of Cr(VI) and NH_4^+ adsorption using greensand (glauconite) as a low-cost adsorbent from aqueous solutions. Water Environ. J. 34, 45–56.
Poo, K.M., Son, E.B., Chang, J.S., Ren, X., Choi, Y.J., Chae, K.J., 2018. Biochars derived from wasted marine macro-algae (*Saccharina japonica* and *Sargassum fusiforme*) and their potential for heavy metal removal in aqueous solution. J. Environ. Manag. 206, 364–372.
Qi, L., Zuo, G., Cheng, Z., Wang, L., Zhou, C., 2013. Treatment of chemical warfare agents by combined sodium percarbonate with tetraacetylethylenediamine solution. Chem. Eng. J. 229, 197–205.
Roberts, D.A., Paul, N.A., Cole, A.J., De Nys, R., 2015. From waste water treatment to land management: conversion of aquatic biomass to biochar for soil amelioration and the fortification of crops with essential trace elements. J. Environ. Manag. 157, 60–68.
Rorrer, G.L., Cheney, D.P., 2004. Bioprocess engineering of cell and tissue cultures for marine seaweeds. Aquacult. Eng. 32, 11–41.
Ruan, X., Sun, Y., Du, W., Tang, Y., Liu, Q., Zhang, Z., Doherty, W., Frost, R.L., Qian, G., Tsang, D.C.W., 2019. Formation, characteristics, and applications of environmentally persistent free radicals in biochars: a review. Bioresour. Technol. 281, 457–468.
Sharma, G., Bhogal, S., Gupta, V.K., Agarwal, S., Kumar, A., Pathania, D., Mola, G.T., Stadler, F.J., 2019. Algal biochar reinforced trimetallic nanocomposite as adsorptional/photocatalyst for remediation of malachite green from aqueous medium. J. Mol. Liq. 275, 499–509.
Shi, Q., Wang, Y., Zhang, X., Shen, B., Wang, F., Zhang, Y., 2020. Hierarchically porous biochar synthesized with $CaCO_3$ template for efficient Hg^0 adsorption from flue gas. Fuel Process. Technol. 199, 106247–106253.
Su, H.M., Chang, Y.L., Huang, W.N., Chen, T.Y., 2014. Development of aquaculture technology of *Agardhiella subulata*. Fish. Res. Inst. Annu. Rep. 28, 2014.
Sudhakar, K., Sudhakar, R., Samykano, M., Azmi, W.H., Ishak, W.F.W., Yusaf, T., 2018. An overview of marine macroalgae as bioresource. Renew. Sustain. Energy Rev. 91, 165–179.
Thivya, J., Vijayaraghavan, J., 2019. Single and binary sorption of reactive dyes onto red seaweed-derived biochar: multi-component isotherm and modeling. Desalination Water Treat 156, 87–95.
Wang, L., Yang, X., Zhang, A., Bidegain, G., Li, R., Na, G., Yuan, X., 2019. Distribution patterns and ecological risk of endocrine-disrupting chemicalsat Qingduizi Bay (China): a preliminary survey in a developing maricultured bay. Mar. Pollut. Bull. 146, 915–920.
Wang, R.Z., Huang, D.L., Liu, Y.G., Zhang, C., Lai, C., Wang, X., Zeng, G.M., Gong, X.M., Duan, A., Zhang, Q., Xu, P., 2019. Recent advances in biochar-based catalysts: properties, applications and mechanisms for pollution remediation. Chem. Eng. J. 371, 380–403.
Wang, S., Shan, R., Wang, Y., Lu, L., Yuan, H., 2019. Synthesis of calcium materials in biochar matrix as a highly stable catalyst for biodiesel production. Renew. Energy 130, 41–49.
Xin, Y., Gao, M., Wang, Y., Ma, D., 2014. Photoelectrocatalytic degradation of 4-nonylphenol in water with WO_3/TiO_2 nanotube array photoelectrodes. Chem. Eng. J. 242, 162–169.
Xu, L.J., Chu, W., Lee, P.H., Wang, J., 2016. The mechanism study of efficient degradation of hydrophobicnonylphenol in solution by a chemical-free technology of sonophotolysis. J. Hazard Mater. 308, 386–393.
Yin, H., Kong, M., Fan, C., 2013. Batch investigations on P immobilization from wastewaters and sediment using natural calcium rich sepiolite as a reactive material. Water Res. 47, 4247–4258.
Yu, K.L., Lau, B.F., Show, P.L., Ong, H.C., Ling, T.C., Chen, W.H., Ng, E.P., Chang, J.S., 2017. Recent developments on algal biochar production and characterization. Bioresour. Technol. 246, 2–11.
Zhou, X., Yang, Z., Luo, Z., Li, H., Chen, G., 2019. Endocrine disrupting chemicals in wild freshwater fishes: species, tissues, sizes and human health risks. Environ. Pollut. 244, 462–468.
Zuo, S., Li, D., Xu, H., Xia, D., 2020. An integrated microwave-ultraviolet catalysis process of four peroxides for wastewater treatment: free radical generation rate and mechanism. Chem. Eng. J. 380, 122434.